



Designing a Broadband Terahertz Half-Wave Plate Using an Anisotropic Metasurface

C. Gandhi¹ · P. Ramesh Babu¹ · K. Senthilnathan¹

Received: 12 January 2019 / Accepted: 5 March 2019 / Published online: 1 April 2019
© Springer Science+Business Media, LLC, part of Springer Nature 2019

Abstract

We design a multi-resonance metasurface at terahertz frequency, which can act as a polarization manipulator in the reflective mode. The proposed polarization converter consists of periodic unit cells and each unit cell has a resonator on the top surface. While a dielectric material forms the middle layer, a gold foil constitutes the bottom layer. The proposed polarization converter converts a linearly polarized terahertz wave into an orthogonal one for a wide range of operating frequencies. It provides a maximum conversion efficiency in the frequency range of 0.64–1.47 THz where the magnitudes of the cross reflection coefficients exceed 90%. The calculated relative bandwidth of the proposed converter is 78.67%. The phase difference of the reflected wave is between -180° and 180° depending upon the operating frequency. Further, based on the detailed numerical results, we corroborate that the proposed device is robust against the variations in the structural parameters. The proposed converter maintains the conversion efficiency for various incident angles from 0° to 30° . Besides, we also demonstrate the possibility of tuning the polarization conversion ratio by integrating silicon in the metasurface. The proposed metasurface may find potential applications in communications, antenna, and radar cross-section reduction technology.

Keywords Polarization converter · Tunable metasurface · Wave-plate · Terahertz frequency

1 Introduction

In recent years, the terahertz technology has gained a special attention as it finds several applications in various disciplines, namely, non-destructive testing, imaging, army target detection, and communications [1–3]. At present, it is well known that

✉ K. Senthilnathan
senthe@gmail.com

¹ Department of Physics, School of Advanced Sciences, Vellore Institute of Technology, Vellore 632014, India

only the limited photonic devices, namely, efficient terahertz sources and extremely sensitive terahertz detectors are available in terahertz technology [4, 5]. Thus, progress of terahertz technology was in slow phase owing to the unavailability of efficient photonic devices to control the terahertz waves. At this juncture, it is worthwhile to mention that the superior functioning optical devices such as lenses, absorbers, sensors, and polarization manipulators are yet to be investigated [6–9]. Very recently, designing of such superior functioning optical devices using an artificial material called metamaterial has been the topic of research in terahertz technology [10]. Metamaterials are defined as an artificial structure-dependent composite materials which respond to the electromagnetic wave in an unconventional way when compared to the natural materials. The fundamental elements of the metamaterial are the meta-atoms, which have the sub-wavelength dimension of the operating wavelength. It is reported that these meta-atoms are capable enough to manipulate the parameters of the electromagnetic wave in the sub-wavelength range [11]. Owing to this special feature of meta-atoms, various novel optical devices, namely, superlens [12], invisibility cloak [13], perfect absorber [14], modulators [15], and polarization converter [16], have been experimentally demonstrated. However, at present, the progress in this technology is slow because of the requirement of complicated resonance structure and challenges in the fabrication process of meta-atoms. To overcome these difficulties, a two-dimensional equivalent of the metamaterial called metasurface (MS) has been proposed. It is to be noted that the electromagnetic properties can be tuned to the desired level through the geometry of the metasurface [17, 18]. Of all the abovementioned optical devices, in this paper, we intend investigating the polarization manipulator.

It is well known that the bi-refringence crystals were used for achieving the polarization rotation of the electromagnetic waves in the transmission type. The polarization rotation of the incident waves take place only when the light passes through the spatial extension which is greater than that of the operating wavelength. Thus, the polarization converters made of conventional materials are bulky in nature. In addition, they also possess poor conversion efficiency and narrow bandwidth for the operating frequency. These drawbacks of the polarization manipulator made of conventional materials have been overtaken by the recent development of metasurface-based polarization manipulators. These polarization converters (PCs) manipulate the phase of the wave in the sub-wavelength range of operation. The significant advantages of the MS-based polarization converters are miniaturized geometry and greater conversion efficiency. Besides, MS-based PCs are capable of covering the various operational range of the electromagnetic spectrum, starting from, microwave, terahertz, infrared to optical frequency. In general, based on the geometry, MS-based polarization converters are classified into two types, namely, an-isotropic resonator for the reflection type conversion [19–25] and chiral structure resonator for the transmission type converter [26–30]. In recent times, the researchers started focusing on designing the PC in the terahertz domain by exploiting the advantages of the MS. Mainly, in this direction, the research work is focused on broadband [23, 24, 31, 32] with the fixed polarization conversion ratio (PCR). Here, the optimized geometry helps to achieve the fixed PCR which may not be optimal from the fabrication point of view. Further, the fixed PCR is also highly undesirable in various practical applications. Thus, an alternative method has been proposed

for tuning the PCR by using the hybridization of conventional materials with the MS. The following materials, namely, graphene [33], silicon [34], and phase change materials [35–37], are utilized for tuning the PCR.

A PC of simple design with ultra-wide bandwidth, compact size, and enhanced efficiency is highly desirable for the practical applications. In this work, we intend to propose a polarization converter with the above mentioned salient features. The paper is laid out as follows. In Section 2, we delineate the geometry of the unit cell of the proposed PC and also discuss the relevant theory. Section 3 discusses the performance of the proposed PC in terms of reflection spectra. In Section 4, we address robustness of the PC against the variations of the structural parameters. We present the physical mechanism of PC with the help of surface current distributions in Section 5. Further, we discuss the integration of the photosensitive material into the MS for achieving tunable PCR in Section 6. Finally, in Section 7, we present the crux of research work presented in this work.

2 Unit Cell Design and Theoretical Analysis

Figure 1a, b illustrates the geometry of the unit cell. The incident electromagnetic wave makes an angle θ with the z -direction. The unit cell comprises of three layers. As was mentioned, the dielectric material is sandwiched between the metasurface-based resonator on the top and the continuous metallic sheet at the bottom. Figure 1c represents the optimized geometrical structure of the proposed unit cell and it has been designed using the CST software based on the finite element method. Here, p is

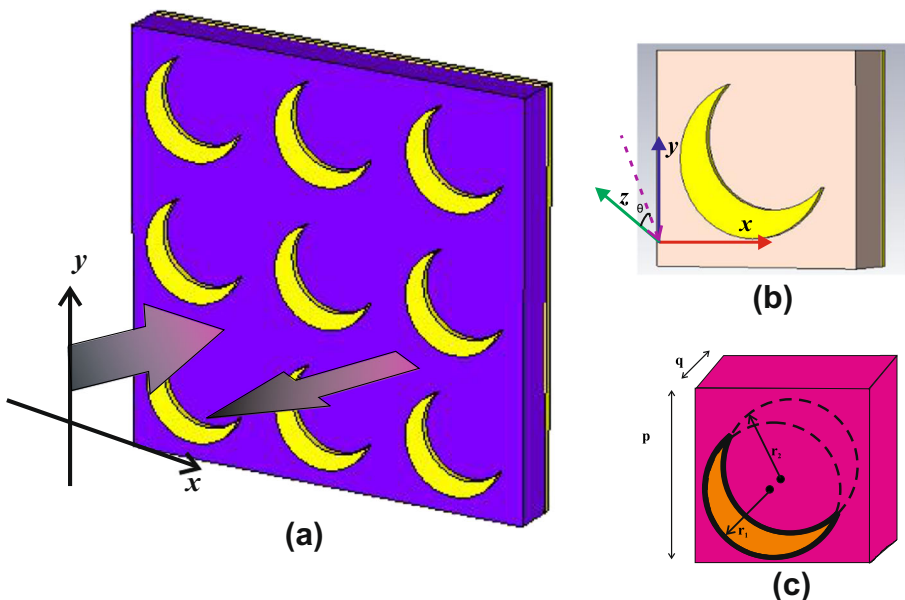


Fig. 1 Geometry of the polarization converter: **a**, **b** crescent geometry and **c** dimension of the unit cell are as follows: $p = 115 \mu\text{m}$, $r_1 = 46 \mu\text{m}$, and $r_2 = 46 \mu\text{m}$, and $q = 37.5 \mu\text{m}$

the periodicity of the unit cell and it is set as $115 \mu m$. The radii of the inner and outer circles are optimized to be $r_1 = 46 \mu m$, and $r_2 = 46 \mu m$, respectively. The thickness of the top as well as the bottom layer is, $s = 0.25 \mu m$ with the electrical conductivity of $\sigma = 5.8 \times 10^7 S/m$. Polyimide is used as a dielectric layer whose thickness is, $q = 37.5 \mu m$ with the permittivity, $\epsilon = 3.5$ and the loss tangent, $\tan \delta$, is 0.02. To extract the scattering parameter, we use the periodic boundary conditions with the floquet ports. The electric field and the magnetic field are oriented parallel to the y - and x -axes, respectively. The continuous metallic plate eliminates the transmission of the electromagnetic wave. Therefore, the co- and cross-polarization reflections have been the dominant processes in the unit cell.

The schematic diagram Fig. 2 describes the conversion mechanism of the converter. As and when the electromagnetic (em) wave enters into PC, the EM wave is split into two components along u - and v -axes by making an angle of 45° with the original field direction. The amplitude and phase of the incident field, \mathbf{E}_i , and the reflected field, \mathbf{E}_r , are written as $\mathbf{E}_i = \mathbf{u}E_{iu}e^{j\phi} + \mathbf{v}E_{iv}e^{j\phi}$, and $\mathbf{E}_r = \mathbf{u}E_{ru} + \mathbf{v}E_{rv} = \mathbf{u}r_uE_{iu}e^{j\phi} + \mathbf{v}r_vE_{iv}e^{j\phi}$, respectively. Using this, the reflection ratios from y -to- y and y -to- x are given as $r_{yy} = |\mathbf{E}_{yr}|/|\mathbf{E}_{yi}|$ and $r_{xy} = |\mathbf{E}_{xr}|/|\mathbf{E}_{yi}|$, respectively. The conversion efficiency of the polarization converter is defined as

$$PCR = \frac{|r_{xy}|^2}{|r_{xy}|^2 + |r_{yy}|^2}. \tag{1}$$

The reflections r_{xy} and r_{yy} are termed as co- and cross-polarization reflection coefficients, respectively. The direction of the polarization rotation is described by η which describes the angle of rotation of the reflected wave. The rotation angle, η ,

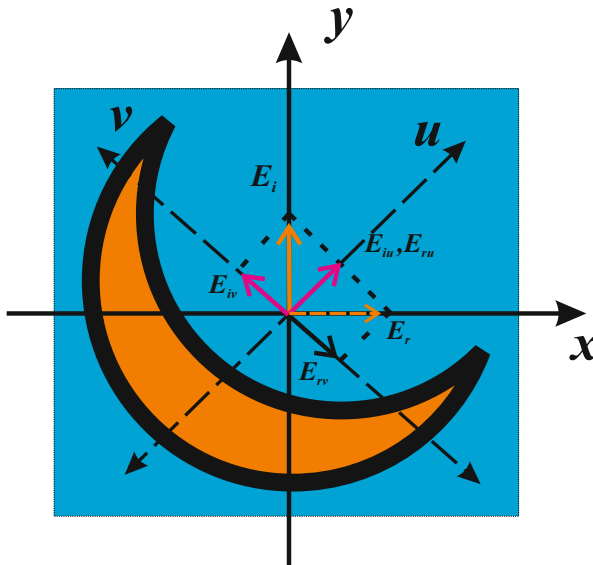


Fig. 2 Schematic diagram represents the conversion mechanism of linearly polarized into orthogonal conversion

is related to the incident and reflected field components by the relation, $\eta = \tan^{-1}(|E_{xr}|/|E_{yr}|)$. The phase difference between the reflected co- and cross-polarization component of the em wave that stems due to anisotropic nature of the metasurface is calculated as $\Delta\phi_{xy} = \arg(\mathbf{r}_{xy}) - \arg(\mathbf{r}_{yy})$. Here, $\Delta\phi_{xy}$ can take the values between $[-180^\circ, 180^\circ]$ depending on the operating frequency.

3 Performance of PC

In this section, we delineate the reflectance of the co- and cross-polarization components. Figure 3 depicts the variation of reflection amplitudes of normalized co- and cross-polarization components for a wide range of frequencies from 0.4 to 1.6 THz. The reflectance of the cross-polarization, $R_{xy}(= |r_{xy}|^2)$, exceeds 90% in the frequency interval from 0.64 to 1.47 THz. On the other hand, the reflectance of co-polarization, $R_{yy}(= |r_{yy}|^2)$, turns below 10% for the said frequency range. Thus, the contribution of cross-polarization reflection is much pronounced. From Fig. 3, it is conspicuous that the reflectance of cross-polarization turns maximum at various resonance frequencies. That is, the observed maximum reflectances are 0.97, 0.96, 0.97, and 0.92 at the resonances of 0.69, 0.96, 1.27, and 1.46 THz, respectively. To get a better insight, the variations in co-polarization reflectance are plotted on logarithmic scale wherein the multiple resonances are observed as shown in Fig. 4. The value of r_{yy} is below -10 dB for the range from 0.64 to 1.47 THz. The magnitude of r_{yy} dips to -33.3 , -57.1 , -41 and -27 dB at the resonance frequencies 0.69, 0.96, 1.27, and 1.46 THz, respectively. Thus, the proposed PC is capable of converting the linearly polarized em wave into orthogonally polarized one (cross-polarization). Here, the cross-polarization reflection is observed to be greater than -3 dB. Besides, we notice an appreciable increment in the conversion efficiency exceeding 90%.

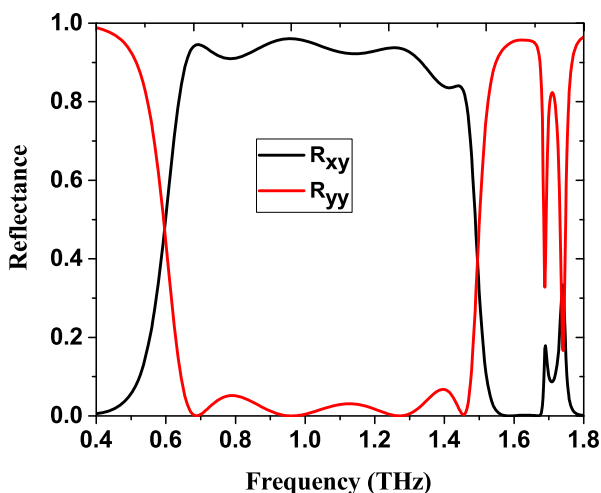


Fig. 3 Reflection amplitude of the designed converter for normal incident wave

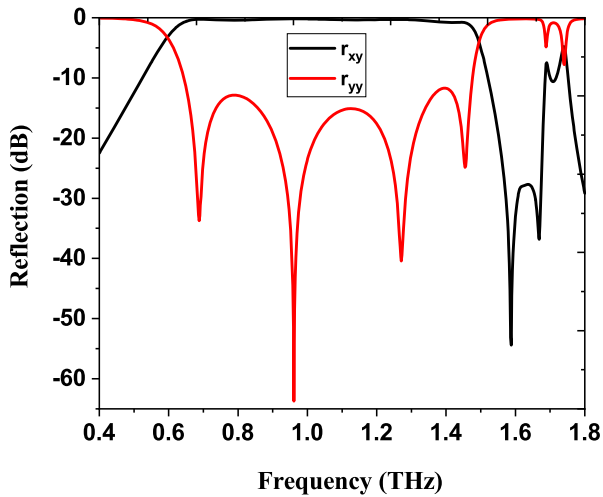


Fig. 4 Simulated co- and cross-polarization reflection

Next, we turn to quantify the performance of the proposed PC by studying the PCR. The conversion power of the device can be studied using Eq. 1. The calculated PCR for the unit cell is shown in Fig. 5. We note that the maximum conversion efficiency is observed for a wide range of frequencies. To be precise, it exceeds 90% for a wide frequency range from 0.64 to 1.46 THz and it is very close to 100% at the resonance frequencies. The relative bandwidth of the proposed converter is given by, $R_{BW} = 2 \times (f_u - f_l) / (f_u + f_l) \times 100\%$, where, f_u and f_l represent the upper and lower frequencies when the conversion efficiency is greater than 90%. The calculated value of the bandwidth is 78.67%.

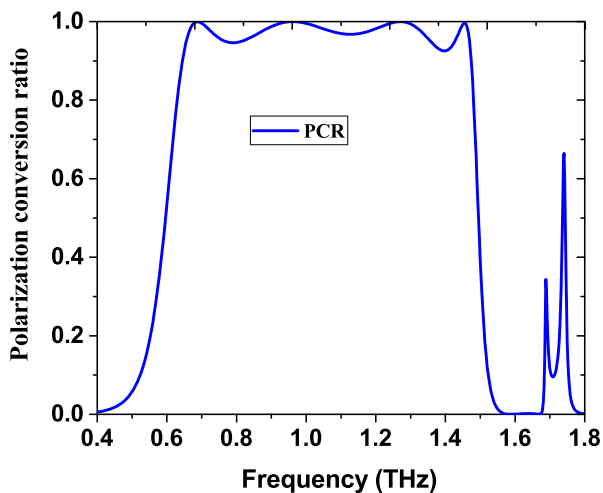


Fig. 5 Polarization conversion ratio of the optimized converter for normal incident with both polarizations

To understand the minimum of co-polarization reflection amplitude for a range from 0.64 to 1.47 THz, we analyze the surface impedance of the PC and the same is defined as

$$Z_{eff}(\omega) = \sqrt{\frac{\mu_{eff}(\omega)}{\varepsilon_{eff}(\omega)}}. \quad (2)$$

Figure 6 shows the real and imaginary parts of the surface impedance of the unit cell. It is clear that the real part of Z_{eff} is close to 1 which, in turn, implies the surface impedance does match with the free space. The imaginary part of the Z_{eff} is almost zero. These two conditions signify that the maximum transmission of incoming wave and minimum reflection in the co-polarized mode.

To confirm that the reflected em wave is in orthogonal state, a plot is drawn between polarization rotation angle, η , against the frequency as displayed in Fig. 7. It may be noted that the reflected em wave makes an angle 90° with the original direction, proving that the reflected light is essentially orthogonal at the resonance frequencies. It is known that the phase difference between the co- and cross-polarized reflected waves plays an indispensable role in determining the state of polarization. To predict the various polarization states and thereby, to identify the nature of wave plates, we compute the phase difference, $\Delta\phi_{xy}$, and its variations are depicted in Fig. 8. From this, we find that $\Delta\phi_{xy}$ is 0° at both the resonance frequencies 0.69 and

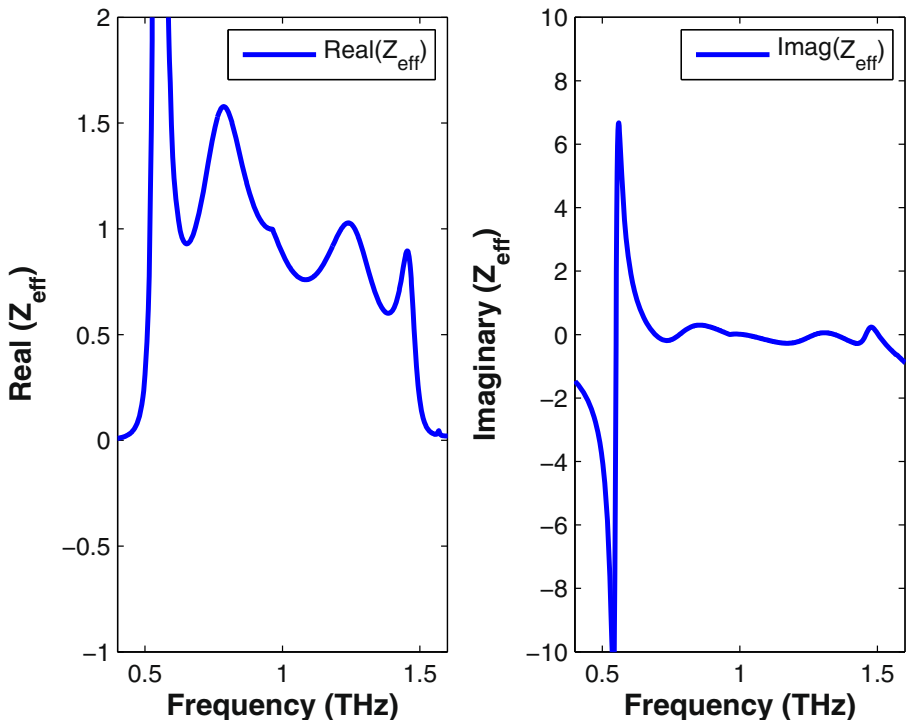


Fig. 6 Surface impedance of the proposed CPC: **a** real part of the impedance and **b** imaginary part of the impedance

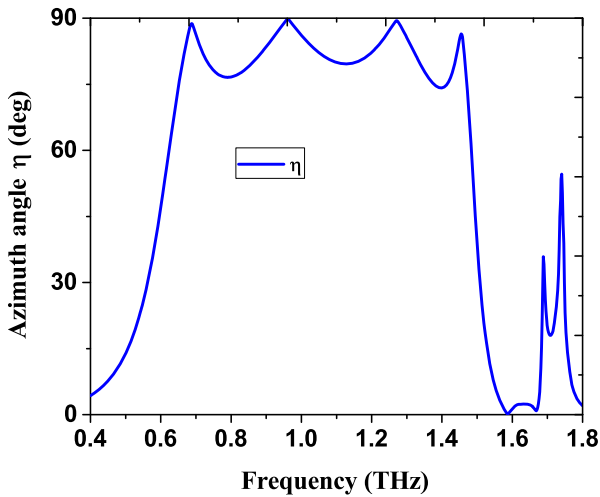


Fig. 7 Polarization rotation angle (η) of the proposed PC in the working frequency

1.27 THz. Hence, the proposed PC acts like a half wave plate (HWP) and it generates linearly polarized wave. Further, $\Delta\phi_{xy}$ turns out to be 180° and -180° at the resonance frequencies 0.96 and 1.46 THz, respectively. These conditions essentially mean the generation of linearly polarized wave. Besides, away from the resonance frequencies, $\Delta\phi_{xy}$ reaches 90° at two different frequency ranges, 0.65–0.66 THz and 0.95–1.2 THz. This results in left elliptically polarized wave as the amplitudes of the co- and cross-polarized components are not equal. Similarly, $\Delta\phi_{xy}$ is -90° in the frequency ranges, 0.7–0.94 THz and 1.27–1.42 THz and it results in a right elliptically polarization. Thus, these studies substantiate that the proposed PC could act as a half wave plate at the resonance frequencies.

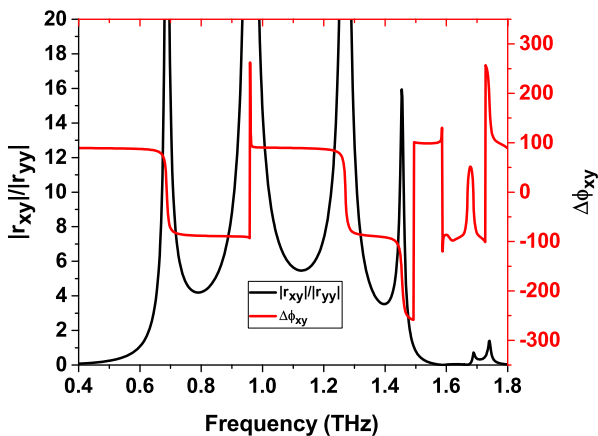


Fig. 8 Phase retardation of the reflected wave at the resonance frequencies between the arguments of the co- r_{xy} and the cross- r_{yy} polarization reflection

So far, we have analyzed the reflective characteristics of the polarization converter along the major axis. To get better understanding of the conversion mechanism, the normal incident y -polarized EM wave can be resolved into two perpendicular components along the u - and v -axes and the corresponding fields are represented by E_{iu} and E_{iv} , respectively, as shown in Fig. 9a and b. The magnitudes of the reflected waves along the u - and v -axes are represented as r_u and r_v , respectively, as illustrated in Fig. 9a. Owing to the diagonal symmetry of the structure, the reflection amplitudes are almost equal ($r_u \approx r_v$). Further, the phase difference between ϕ_u and ϕ_v is 180° . Here, we assume that the direction of the u -component of the field remains the same for both incident and reflected components. However, the v -component of the electric field gets reversed along negative v axis. Consequently, the resultant field appears in x -direction. As portrayed in the Fig. 9b, the phase difference is nearly 180° in the operating frequency range from 0.69 to 1.56 THz. Thus, this mechanism ensures 90° rotation of the incident electric field.

4 Variations of PCR Against Structural Parameters

It is well known that metamaterials are structure-dependent electromagnetic materials. Thus, the resonance frequency, reflection spectra, bandwidth, and polarization conversion efficiency of these materials are dependent on the structural parameters. Thus, it is essential to analyze the PCR by varying the various geometrical parameters of unit cell. In this section, we study the PCR by varying the following structural parameters, namely, periodicity, p , dielectric thickness, q , and inner, r_1 , and outer, r_2 , radii of the metasurface. First, we investigate the influence of the periodicity of the unit cell by keeping the other three geometrical parameters as a constant. As shown in Fig. 10a, we find that the PCR almost remains the same when the periodicity of the unit cell is varied from the optimized value. However, the bandwidth increases (decreases) minimally when p is decreased (increased) and

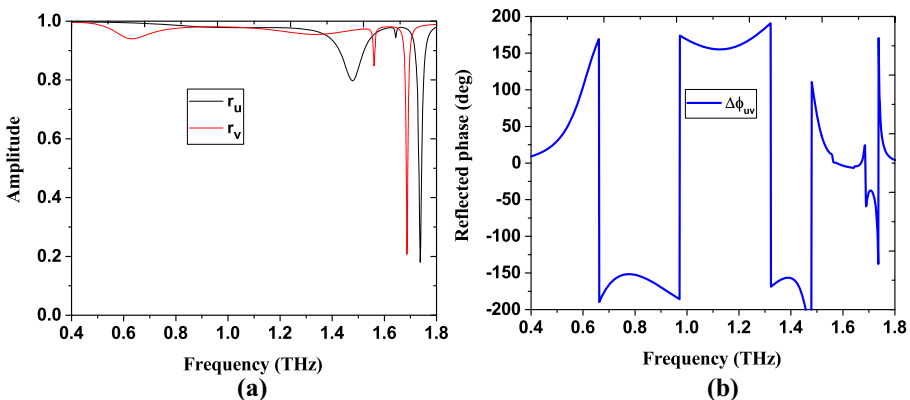


Fig. 9 Reflection spectra along the u - and v -axes: **a** the amplitude of r_u and r_v , **b** the phase difference $\Delta\phi_{uv}$ generated by the anisotropic geometry

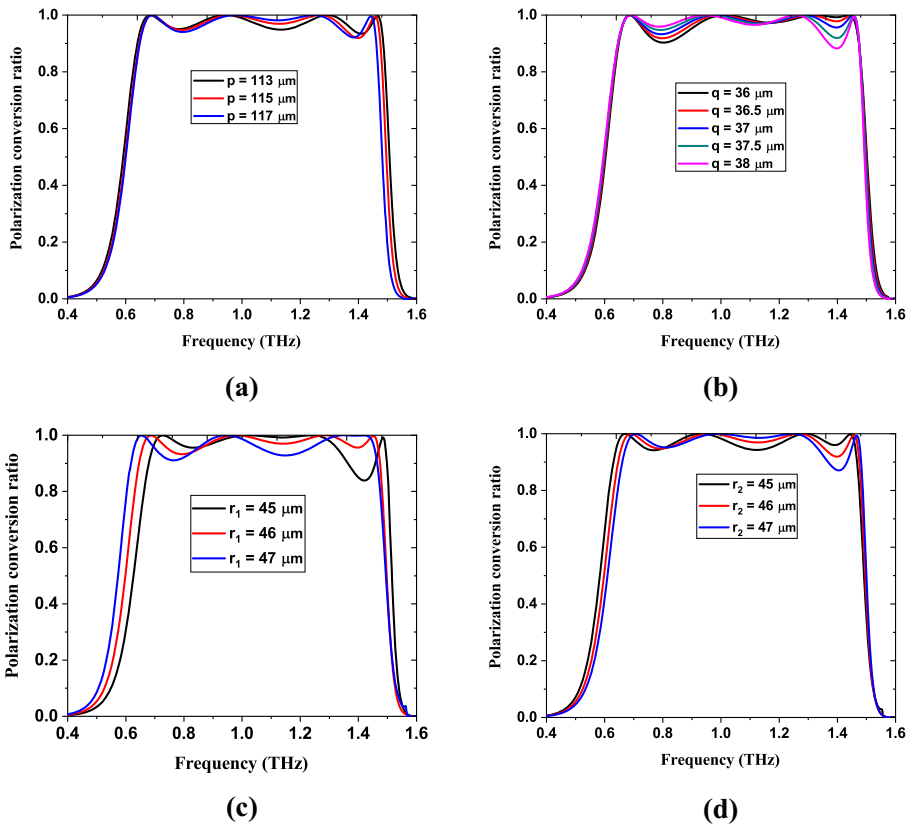


Fig. 10 The analysis of PCR over various geometrical parameters: **a** periodicity of the unit cell (p); **b** dielectric layer thickness (q); **c** outer radius of the metasurface (r_1); **d** inner radius of the metasurface (r_2)

accordingly the resonance frequency gets shifted. When the dielectric thickness is varied, the bandwidth remains the same but the PCR varies within the permissible level as illustrated in Fig. 10b. Next, we discuss the role of inner and outer radii. From Fig. 10c, it is very clear that PCR decreases to 84% when the outer radius, r_1 , is decreased from the optimized value. Here, the change in the bandwidth is also minimum. We find that both the bandwidth and PCR do not change appreciably when the inner radius is varied as shown in Fig. 10d. These numerical studies corroborate that the proposed device is highly robust against the variations in the structural parameters.

From the above studies, it is very clear that the proposed PC would act as a HWP only for normal incidence. In what follows, we would like to center our argument on the capability of the proposed PC holding its role as HWP for angles other than normal incident angle. Thus, the wide angle operation is a desirable attribute for all practical applications. Now, we proceed to analyze the angular sensitivity of the PCR. Figure 11 represents the response of the PCR for various incident angles, (θ), from 0° to 80° . Here, PCR is within the permissible level up to 30° but it decreases drastically

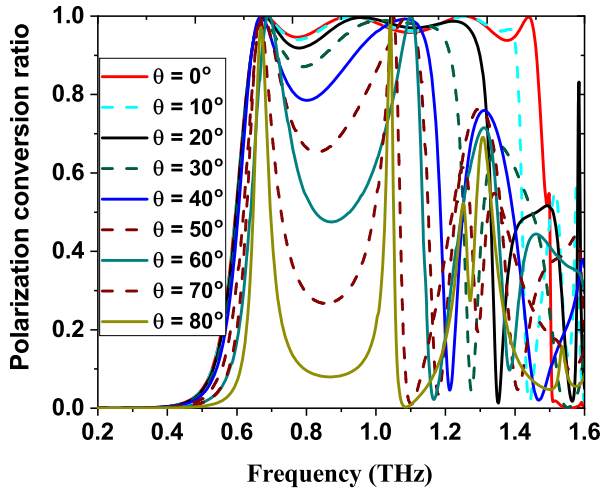


Fig. 11 Polarization conversion ratio of the MS with various incidence angles

if the angle is further increased. Besides, the bandwidth of PCR shrinks to dual band beyond 30° .

Finally, we study the role of dielectric loss tangent which turns out to be an important figure of merit of PC. It is basically a ratio of imaginary and real part of the dielectric constant. Here, we consider the polyimide layer as a dielectric material as we mentioned earlier. Figure 12 shows the conversion efficiency with various loss tangents. The analysis shows that the conversion efficiency decreases when $\tan \delta$ is increased. Hence, in order to catch up with a better conversion efficiency, the dielectric loss must as low as possible.

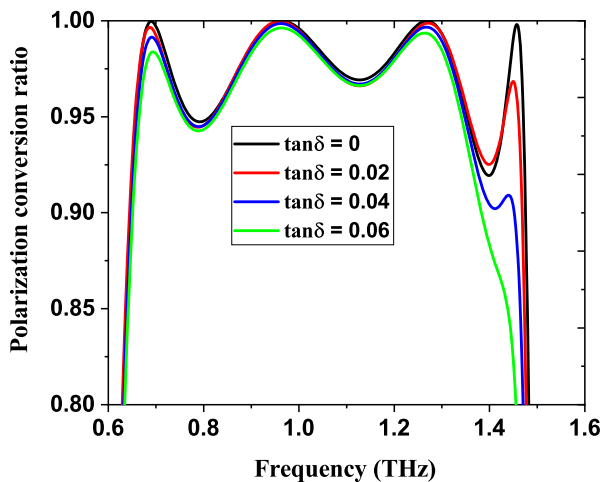


Fig. 12 Polarization conversion ratio as a function of dielectric loss tangent

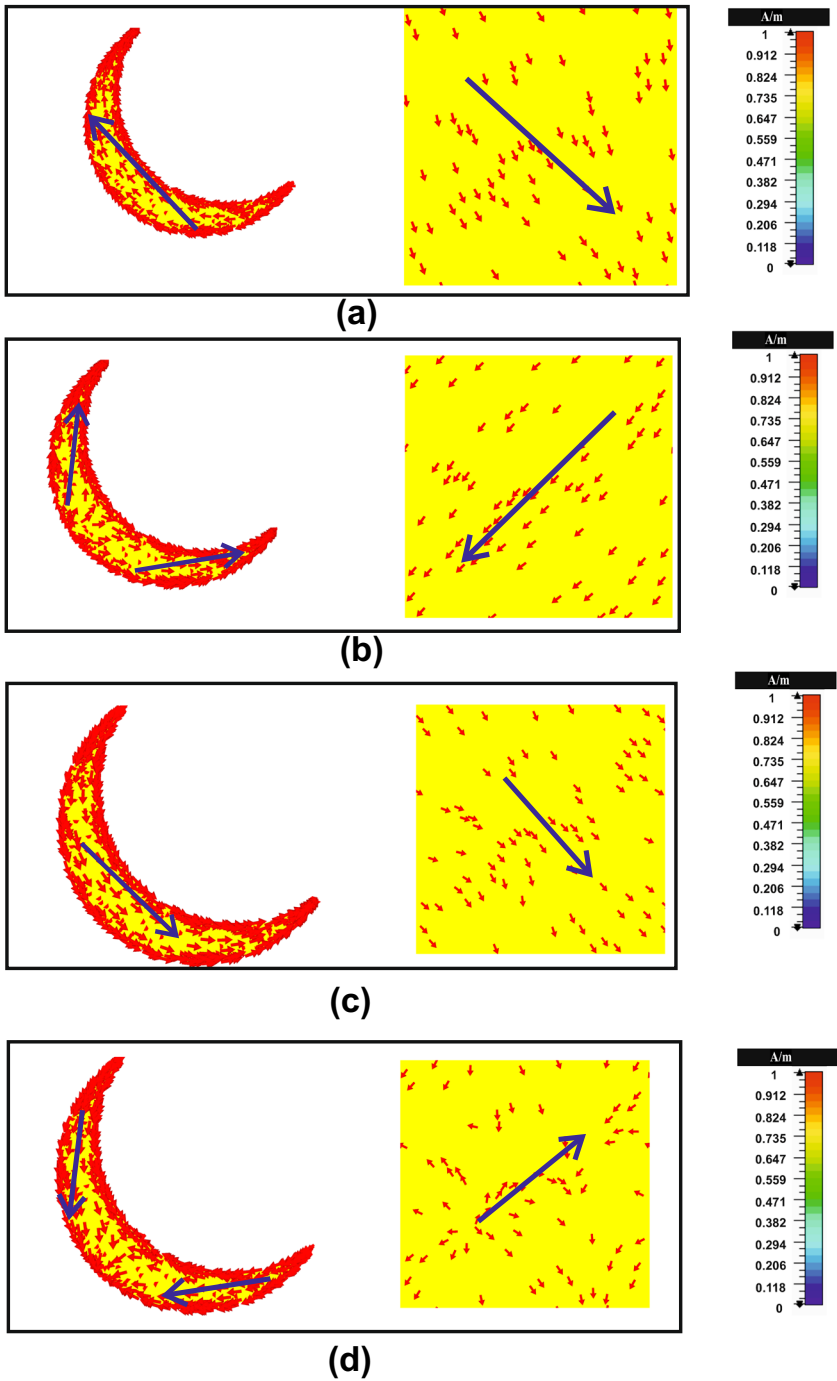


Fig. 13 Surface current distribution on the MS and the bottom plate at resonant frequencies: **a** 0.69 THz, **b** 0.96 THz, **c** 1.27 THz, and **d** 1.46 THz

5 Physical Mechanism

Having understood the performance of ultra-wideband polarization rotator, the next step is to analyze the physical process in terms of the surface current flow. Figure 13a–d portrays the surface current distributions on the top and bottom layers at four resonant frequencies of 0.69, 0.96, 1.27, and 1.46 THz, respectively. We find that the surface current on the top layer is anti-parallel with the bottom layer at the resonance frequencies of 0.69 THz, 0.96 THz, and 1.46 THz. Thus, the magnetic resonance is responsible for the polarization conversion at these resonance frequencies. On the other hand, the surface current on the top layer is parallel to that in the bottom layer at a resonance frequency of 1.27 THz. Here, electric resonance takes care of the polarization conversion process. Thus, these four resonance frequencies play a crucial role in achieving high efficiency ultrabroadband polarization conversion.

6 Tunable PCR

As has been discussed in the introduction section, PCR is fixed for most of the PCs. However, it is necessary to tune the PCR for various applications. Based on the above discussion, one can infer that the proposed PC provides only the fixed PCR. In this section, to understand the controllable polarization conversion, Si, which is essentially a photo-conductive material, is integrated in MS as shown in Fig. 14. Here, we consider the Si with the permittivity, ϵ being 11.9. It is well established that the Si

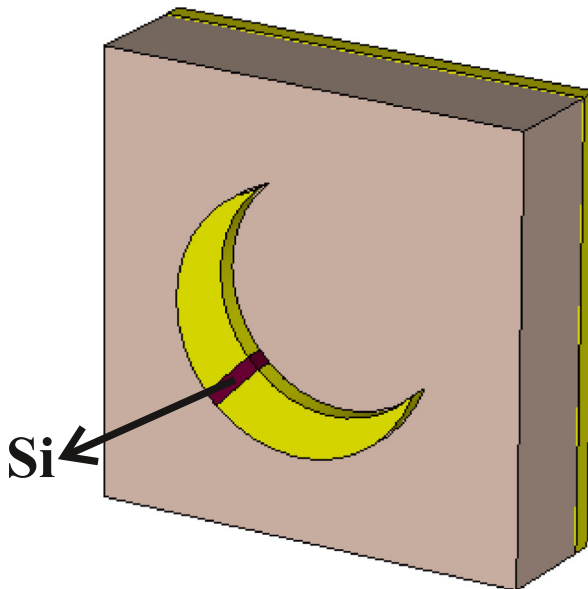


Fig. 14 Geometrical description of the tunable PCR metasurface

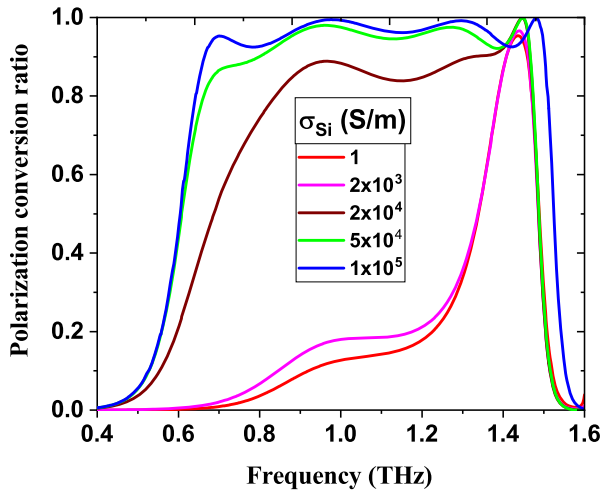


Fig. 15 PCR tunable as a function of electrical conductivity of the Silicon

acts as an insulator in the absence of optical pump and it becomes a conductor at high intensity [34, 38–40]. This phase transition plays an indispensable role in the polarization conversion. Figure 15 shows the variation of PCR with the variation of the electrical conductivity of Si σ_{Si} . As mentioned earlier, the photo-dependent material, Si acts as an insulator when there is no laser light illumination and its electrical conductivity σ_{Si} is 1 S/m. The bandwidth of PCR is narrow as the generation of the photo electrons is less in the insulating state. On the other hand, with the high pump power, the bandwidth turns out to be maximum with greater efficiency when the conductivity increases from 1 to 1×10^5 S/m. From this analysis, it is very clear that the bandwidth and the PCR are controllable when Si changes from insulating to the conducting state.

7 Conclusion

We have designed a multi-resonance metasurface that could act as a polarization converter at terahertz frequency in the reflective mode. The proposed polarization converter has been able to convert a linearly polarized THz wave into an orthogonal one for a wide range of operating frequencies. Further, it provides a maximum conversion efficiency in the frequency range of 0.64–1.46 THz where the magnitudes of the cross reflection coefficients exceed 90%. The calculated relative bandwidth of the proposed converter is 78.67%. Then, we have carried out a detailed numerical analysis to claim that the proposed device is robust against the variations in the structural parameters. Further, we have also demonstrated the possibility of tuning the polarization conversion ratio by integrating silicon metasurface. Thus, it is envisaged that the proposed polarization converter may draw wide attention in various fields, especially, in communications, antenna and radar cross-section reduction technology.

References

1. C.D. Stoik, M.J. Bohn, J.L. Blackshire, *Optics Express* **16**(21), 17039 (2008).
2. J.F. Federici, B. Schulkin, F. Huang, D. Gary, R. Barat, F. Oliveira, D. Zimdars, *Semiconductor Science and Technology* **20**(7), S266 (2005).
3. R. Piesiewicz, T. Kleine-Ostmann, N. Krumbholz, D. Mittleman, M. Koch, J. Schoebei, T. Kurner, *IEEE Antennas and Propagation Magazine* **49**(6), 24 (2007).
4. J. Dai, J. Liu, X.C. Zhang, *IEEE Journal of selected topics in Quantum Electronics* **17**(1), 183 (2011).
5. F. Blanchard, G. Sharma, L. Razzari, X. Ropagnol, H.C. Bandulet, F. Vidal, R. Morandotti, J.C. Kieffer, T. Ozaki, H. Tiedje, et al., *IEEE Journal of Selected Topics in Quantum Electronics* **17**(1), 5 (2011).
6. A. Siemion, A. Siemion, M. Makowski, J. Suszek, J. Bomba, A. Czerwiński, F. Garet, J.L. Coutaz, M. Sypek, *Optics Letters* **37**(20), 4320 (2012).
7. W.D. Furlan, V. Ferrando, J.A. Monsoriu, P. Zagrajek, E. Czerwińska, M. Szustakowski, *Optics Letters* **41**(8), 1748 (2016).
8. J. Liu, J. Dai, S.L. Chin, X.C. Zhang, *Nature Photonics* **4**(9), 627 (2010).
9. L. Deng, J. Teng, L. Zhang, Q. Wu, H. Liu, X. Zhang, S. Chua, *Applied Physics Letters* **101**(1), 011101 (2012).
10. C.R. Simovski, P.A. Belov, A.V. Atrashchenko, Y.S. Kivshar, *Advanced Materials* **24**(31), 4229 (2012).
11. J.B. Pendry, A.J. Holden, D.J. Robbins, W. Stewart, *IEEE transactions on microwave theory and techniques* **47**(11), 2075 (1999).
12. J.B. Pendry, *Physical Review Letters* **85**(18), 3966 (2000).
13. D. Schurig, J. Mock, B. Justice, S.A. Cummer, J.B. Pendry, A. Starr, D. Smith, *Science* **314**(5801), 977 (2006).
14. N.I. Landy, S. Sajuyigbe, J. Mock, D. Smith, W. Padilla, *Physical Review Letters* **100**(20), 207402 (2008).
15. H.T. Chen, W.J. Padilla, M.J. Cich, A.K. Azad, R.D. Averitt, A.J. Taylor, *Nature photonics* **3**(3), 148 (2009).
16. N.K. Grady, J.E. Heyes, D.R. Chowdhury, Y. Zeng, M.T. Reiten, A.K. Azad, A.J. Taylor, D.A. Dalvit, H.T. Chen, *Science* p. 1235399 (2013).
17. N. Yu, P. Genevet, M.A. Kats, F. Aieta, J.P. Tetienne, F. Capasso, Z. Gaburro, *Science* p. 1210713 (2011).
18. Y. Yang, W. Wang, P. Moitra, I.I. Kravchenko, D.P. Briggs, J. Valentine, *Nano Letters* **14**(3), 1394 (2014).
19. J. Hao, Y. Yuan, L. Ran, T. Jiang, J.A. Kong, C. Chan, L. Zhou, *Physical Review Letters* **99**(6), 063908 (2007).
20. Y. Jia, Y. Liu, W. Zhang, S. Gong, *Applied Physics Letters* **109**(5), 051901 (2016).
21. L. Zhang, P. Zhou, H. Lu, L. Zhang, J. Xie, L. Deng, *Optical Materials Express* **6**(4), 1393 (2016).
22. Q. Lévesque, M. Makhsiyani, P. Bouchon, F. Pardo, J. Jaeck, N. Bardou, C. Dupuis, R. Haïdar, J.L. Pelouard, *Applied Physics Letters* **104**(11), 111105 (2014).
23. Y. Jiang, L. Wang, J. Wang, C.N. Akwuruoha, W. Cao, *Optics Express* **25**(22), 27616 (2017).
24. R. Xia, X. Jing, X. Gui, Y. Tian, Z. Hong, *Optical Materials Express* **7**(3), 977 (2017).
25. W. Zhu, R. Yang, Y. Fan, Q. Fu, H. Wu, P. Zhang, N.H. Shen, F. Zhang, *Nanoscale* (2018).
26. R. Singh, E. Plum, W. Zhang, N.I. Zheludev, *Optics Express* **18**(13), 13425 (2010).
27. J. Zhou, D.R. Chowdhury, R. Zhao, A.K. Azad, H.T. Chen, C.M. Soukoulis, A.J. Taylor, J.F. O'Hara, *Physical Review B* **86**(3), 035448 (2012).
28. J.K. Gansel, M. Thiel, M.S. Rill, M. Decker, K. Bade, V. Saile, G. von Freymann, S. Linden, M. Wegener, *Science* **325**(5947), 1513 (2009).
29. X. Ma, C. Huang, M. Pu, C. Hu, Q. Feng, X. Luo, *Optics Express* **20**(14), 16050 (2012).
30. C. Han, E.P. Parrott, E. Pickwell-MacPherson, *IEEE Journal of Selected Topics in Quantum Electronics* **23**(4), 1 (2017).
31. Y.Z. Cheng, W. Withayachumnankul, A. Upadhyay, D. Headland, Y. Nie, R.Z. Gong, M. Bhaskaran, S. Sriram, D. Abbott, *Applied Physics Letters* **105**(18), 181111 (2014).
32. X.F. Zang, S.J. Liu, H.H. Gong, Y. Wang, Y.M. Zhu, *JOSA B* **35**(4), 950 (2018).
33. W. Zhang, J. Jiang, J. Yuan, S. Liang, J. Qian, J. Shu, L. Jiang, *OSA Continuum* **1**(1), 124 (2018).
34. J. Zhao, Y. Cheng, Z. Cheng, *IEEE Photonics Journal* **10**(1), 1 (2018).

35. T. Lv, Y. Li, H. Ma, Z. Zhu, Z. Li, C. Guan, J. Shi, H. Zhang, T. Cui, *Scientific Reports* **6**, 23186 (2016).
36. X. Zheng, Z. Xiao, X. Ling, *Plasmonics* **13**(1), 287 (2018).
37. Z. Xiao, H. Zou, X. Zheng, X. Ling, L. Wang, *Optical and Quantum Electronics* **49**(12), 401 (2017).
38. N.H. Shen, M. Massaouti, M. Gokkavas, J.M. Manceau, E. Ozbay, M. Kafesaki, T. Koschny, S. Tzortzakis, C.M. Soukoulis, *Physical Review Letters* **106**(3), 037403 (2011).
39. M. Gupta, Y.K. Srivastava, R. Singh, *Advanced Materials* **30**(4), 1704845 (2018).
40. M. Manjappa, Y.K. Srivastava, L. Cong, I. Al-Naib, R. Singh, *Advanced Materials* **29**(3), 1603355 (2017).

Publisher's Note Springer Nature remains neutral with regard to jurisdictional claims in published maps and institutional affiliations.